Deciphering the Exceptional Selectivity of Semipinacol Rearrangements in Cis-Fused β-Lactam Diols Using High-Level Quantum Chemical Methods

Abdulkader Baroudi[†,*] and Amir Karton[‡,*]

[†] College of Engineering and Technology, American University of the Middle East, Kuwait.

[‡] School of Molecular Sciences, The University of Western Australia, Perth, WA 6009, Australia.

Abstract

The mechanism for the semipinacol rearrangement in cis-fused β-lactam diols has been examined using highly accurate double-hybrid density functional theory methods. This reaction involves a competition between two possible migrating groups (alkyl and acyl), which can undergo a 1,2 C–C bond migration. We find that acyl migration is both kinetically and thermodynamically more favorable. These results are consistent with experimental observations and are rationalized based on conformational, structural, and orbital interactions analysis. We proceed to investigate the semipinacol rearrangement in trans-fused β-lactam diol and propose that this system undergoes a reversed selectivity which favors the alkyl migration.

Keywords: Semipinacol rearrangement, Reaction mechanism, Computational chemistry, Density functional theory.

Cite as:
A. Baroudi, A. Karton, *Org. Chem. Front.* 6, 725–731 (2019). https://doi.org/10.1039/C8QO01092G

*Corresponding authors. Emails: abdulkader.baroudi@aum.edu.kw, amir.karton@uwa.edu.au

Introduction

Semipinacol rearrangement reactions are an extremely useful tool in organic synthesis for C–C bond migration.[1] Many examples have been published presenting the 1,2-migration of a C–C bond in conjunction with a variety of different leaving groups.[2] Figure 1 gives a schematic representation of this reaction. An important feature of such rearrangements is the presence of more than one possible migrating group (R_1 and R_2, Figure 1) adjacent to the leaving group (L), and thus, more than one possible product can be formed. In addition, the migrating R group can be not only alkyl, but also vinyl, acyl, or aryl migrating groups.[1,2] Hence, a competition in the migration of the two groups R_1 and R_2 would be expected especially when they are of different types, e.g., R_1 = alkyl and R_2 = acyl.[2,3] In a recent study, Grainger *et al.*[4] reported the synthesis of the 6-azabicyclo[3.2.1]octane ring system from the phosphorane and sulfite of cis-fused β-lactam diol. This reaction scheme is illustrated in Figure 2. They found that the semipinacol rearrangement of the β-lactam ring proceeds exclusively through the migration of the *N*-acyl group with no formation of the *N*-alkyl migration product. Nevertheless, to the best of our knowledge a detailed computational study of this high selectivity has not been reported. In the present work, we use highly accurate quantum chemical methods to elucidate the molecular mechanism underlying this process in order to shed light on its remarkable selectivity.

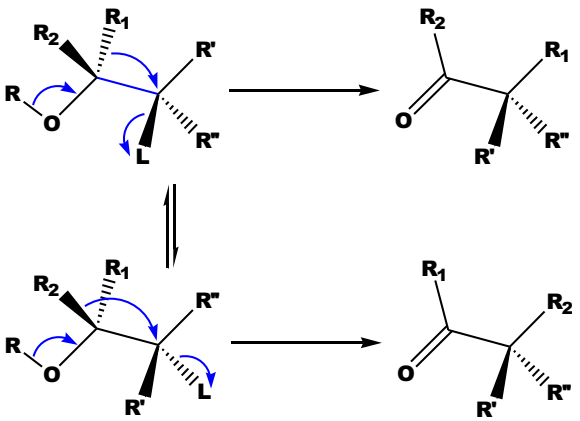

Figure 1. Schematic Representation of Semipinacol Rearrangement Pathways Based on Conformational Change.

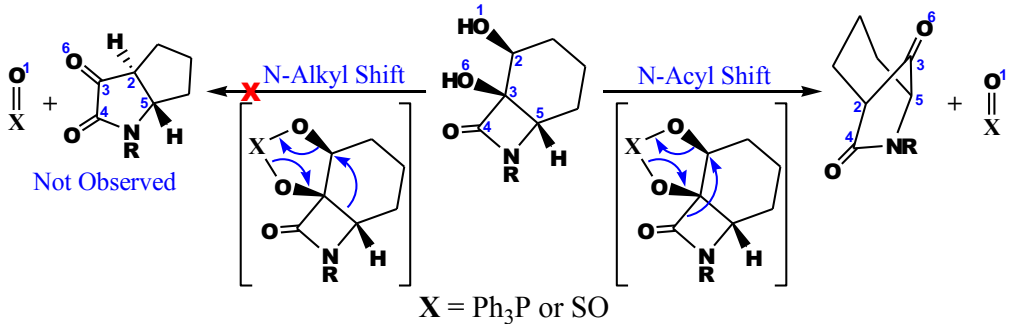

Figure 2. Semipinacol Rearrangement Via Selective N-Acyl Shift of Cis-Fused β-Lactam Diol. Based on Conditions, X is Ph_3P for Phosphorane and SO for Sulfite.

Computational Details

The geometries of all structures were optimized using the B3LYP-D3 exchange-correlation density functional theory (DFT) functional[5,6,7] in conjunction with the 6-31G(2df,p) Pople-style basis set.[8,9] Empirical D3 dispersion corrections[10,11] were included using the Becke–Johnson[12] damping potential (denoted by the suffix -D3).[13] Bulk solvent effects were included using the charge-density-based SMD continuum solvation model.[14] The resulting level of theory

is denoted SMD-B3LYP-D3/6-31G(2df,p). Harmonic vibrational analyses were performed at the same level of theory to confirm each stationary point as either an equilibrium structure (i.e. all real frequencies) or a transition structure (i.e. with one imaginary frequency). The connectivity of the local minima and first-order saddle points was confirmed by performing intrinsic reaction coordinate calculations.[15,16]

High-level double-hybrid density functional theory (DHDFT) calculations[17] were performed in order to obtain accurate electronic energies for the equilibrium and transition structures located along the reaction pathways considered in the present work. Double-hybrid DFT procedures involve both Hartree–Fock-like exchange and MP2-like correlation from second-order Møller–Plesset perturbation theory. These procedures have been found to produce thermochemical properties (such as reaction energies and barrier heights) with mean absolute deviations (MADs) approaching the threshold of 'chemical accuracy' (arbitrarily defined as 1 kcal mol^{-1} ≈ 4.2 kJ mol^{-1}) from a wide range of accurate experimental or theoretical thermochemical determinations.[17,18,19,20,21,22,23,24,25,26] In the present work, we use the spin-component-scaled DSD-PBEP86-D3 DHDFT functional of Kozuch and Martin[18,19] in conjunction with the Def2-TZVPP basis set of Weigend and Ahlrichs.[27] We note that for the smallest system with X = SO (Figure 2) we were able to calculate the potential energy surfaces for the alkyl and acyl shifts using the high-level G4(MP2) composite method.[28,29] The differences (in absolute value) between the G4(MP2) and DSD-PBEP86-D3/Def2-TZVPP reaction energies and barrier heights range between 1.3 and 3.4 kJ mol^{-1} in all cases. This close agreement between the two methods increases our confidence in the DSD-PBEP86-D3/Def2-TZVPP reaction energies barrier heights.

The DSD-PBEP86-D3 electronic energies were converted to Gibbs-free energies at 298 K (ΔG_{298}) using zero-point vibrational energies and thermal corrections obtained at the SMD-

B3LYP-D3/6-31G(2df,p) level of theory. Corrections for bulk solvent effects (CH_3CN for phosphorane and Ph_2O for sulfite)[4] were added to the gas-phase ΔG_{298} values using the SMD model at the M05-2X/6-31G(d) level of theory[30] as recommended by Marenich, Cramer, and Truhlar.[14] All the DFT and DHDFT calculations were carried out with the Gaussian 09 and Gaussian 16 program suites, respectively.[31,32]

Results and Discussion

A concerted semipinacol rearrangement mechanism is believed to require a structural alignment close to anti-conformation between the leaving group (O1—C2 bond) and the migrating group (C3—C4 for acyl migration or C3—C5 for alkyl migration).[1] Figure 3 illustrates these bonds alignments. For simplicity, we will designate the shifts by 'acyl' for *N*-acyl and 'alkyl' for *N*-alkyl. We begin by checking the relative energies of the two conformers that correspond to the two shifts shown in Figure 3. Table 1 depicts the relative Gibbs-free energies of the possible starting conformers. In all cases conformer A is more stable than conformer B. When the substituent X is H or SO (entries 1, 3, and 4, Table 1) conformer A is more stable by up to 1.0 kcal mol^{-1}. However, when X is Ph_3P (entry 2, Table 1) the Gibbs-free energy difference between the two conformers reaches 2.7 kcal mol^{-1}. This result is significant since for X = Ph_3P the difference in activation energy for the alkyl and acyl migrations is similar to the energy difference between the two conformers (*vide infra*).

A closer inspection of the starting conformers shows higher torsion angle O1C2C3C4 in conformer B (α_{r_B}) compared to O1C2C3C5 in conformer A (β_{r_A}), particularly in the case of the sulfites (e.g. 153.1° vs. 128.5°, respectively, Table 1, entry 3). This result supports the preference of acyl over alkyl migration since conformer B is geometrically closer to an anti-periplanar

conformation, and thus, lower angular distortion would be needed in conformer B to form the acyl shift transition structure (TS). However, one should also consider the degree of anti-periplanar alignment in the transition state structure of each reaction pathway.

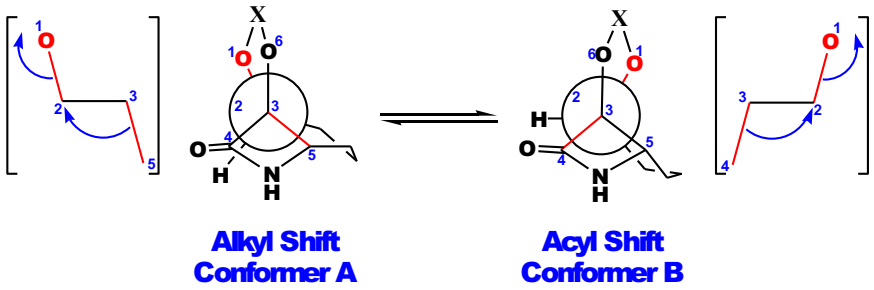

Figure 3. Newman Projections (Through the C2—C3 Bond) of the Starting Conformers that Correspond to Each of the Two Possible Semipinacol Rearrangement Pathways.

Table 1. Relative Gibbs-Free Conformational Energies at 298 K for the Reactants Shown in Figure 3.

	X	Conformer	O1C2C3C4 (α_r)[b]	O1C2C3C5 (β_r)[b]	ΔG_{conf}[d] (kcal mol^{-1})
1	H[a]	A	113.0	151.9	1.0
		B	165.8	97.2	
2	Ph_3P	A	114.7	149.0	2.7
		B	151.8	105.5	
3	SO-I[c]	A	131.6	128.5	0.3
		B	153.1	104.5	
4	SO-II[c]	A	125.9	134.2	0.7
		B	149.5	107.4	

[a] Corresponds to starting diol where intramolecular hydrogen bonding occurs between the two hydroxyl groups.
[b] α_r and β_r are torsion angles in the reactants.
[c] Diastereomers of sulfite (see Figure 4 below).
[d] $\Delta G_{conf} = G_{298}$[B] – G_{298}[A] (a positive sign indicates that conformer A is more stable on the ΔG_{298} energy surface).

A qualitative schematic representation of the reaction profile for the alkyl and acyl migration pathways in the concerted semipinacol rearrangement is given in Figure 4, whilst the

Gibbs-free activation and reaction energies are given in Table 2. The following structural differences between the TSs for the two shifts are noted. Firstly, irrespective of the X-containing ring the TSs of both shifts adopt a tricyclic arrangement. While the alkyl shift assumes a 3, 4, 5-membered fused rings structure, the acyl shift assumes a 3, 4, 6-membered fused rings structure. Thus, TS_{Acyl} involves less ring strain energy and is therefore lower in energy. Secondly, with respect to the cyclohexane skeleton, the bond migration (denoted by the 3-membered dotted ring in the TS) in the alkyl shift is "endo" (C3—C5) versus "exo" in acyl shift (C3—C4), again this structural difference indicates that TS_{Acyl} should be lower in energy.

The acyl shift is both kinetically and thermodynamically more favorable with both cyclic phosphorane and sulfite substrates (Table 2). This preference of acyl migration agrees with the torsion angles analysis discussed above. The acyl shift activation barriers with the phosphorane and sulfite groups are comparable ($\Delta G^{\ddagger}_{298}$ = 33.3 and 33.8 kcal mol^{-1}, respectively). This is somewhat surprising since the two X groups (Ph_3P and SO) have inherently different electronic and steric properties. We believe that this is a result of opposing effects, which overall result in similar activation barriers. For example, as shown in Table 2, a higher torsion angle $\alpha_{TS_{Acyl}}$ in phosphorane (176.4°, entry 1) compared to that of sulfite (166.8°, entry 2) would have accounted for a lower rearrangement barrier of phosphorane due to a more effective orbital alignment that results in transition structure stabilization. Nevertheless, as shown in Table 3, a higher degree of angular distortion ($\alpha_{TS_{Acyl}} - \alpha_{r_B}$) needed for the formation of TS_{Acyl} in phosphorane (24.6°, entry 1) compared with that in sulfite (13.7°, entry 2) would have accounted for higher rearrangement barrier of phosphorane. On the other hand, the above factors seem not to completely counter each other in the case of the alkyl shift reaction pathway. As shown in Table 2, the alkyl shift activation barrier in phosphorane (38.3 kcal mol^{-1}) is noticeably lower than that in sulfite (46.7

kcal mol^{-1}). Similarly, the higher torsion angle $\beta_{TS_{Alkyl}}$ in sulfite (173.8°, entry 2) compared to that of phosphorane (168.4°, entry 1) would have accounted for a lower reaction barrier for sulfite. However, the significantly large degree of angular distortion ($\beta_{TS_{Alkyl}} - \beta_{r_A}$) required for the formation of TS_{Alkyl} in sulfite (45.3°, Table 3, entry 2) surely surpasses the counter effect of high torsion angle $\beta_{TS_{Alkyl}}$ and accounts for the higher alkyl shift activation barrier. It should be mentioned that the reaction barriers for the acyl shift of 33–35 kcal mol^{-1} can readily be overcome under the high-temperature reaction conditions used by Grainger *et al.*[4]

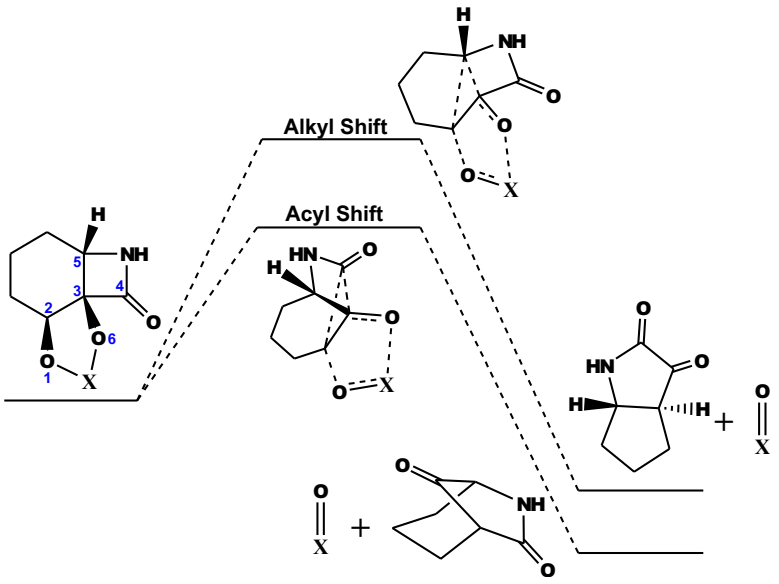

Figure 4. Schematic Potential Gibbs-Free Energy Profiles for the Alkyl and Acyl Migration Pathways in the Concerted Semipinacol Rearrangement. The Gibbs-Free Energies (ΔG_{298}) of the Transition Structures and Products are Given in Table 2.

Table 2. Gibbs free Reaction Energies and Barrier Heights, and TS Torsion Angles (α_{TS} and β_{TS}) for Alkyl and Acyl Migration Pathways.

	X	Shift	$\Delta G^{\ddagger}_{298}$	$\Delta G_{298_{rxn}}$	O1C2C3C4 α_{TS}	O1C2C3C5 β_{TS}	$\Delta\Delta G^{\ddagger a}$
1	Ph_3P	Alkyl	38.3	-28.8	96.3	168.4	5.0
		Acyl	33.3	-41.5	176.4	103.1	
2	SO-I	Alkyl	46.7	-17.0	113.3	173.8	12.9
		Acyl	33.8	-27.8	166.8	115.2	
3	SO-II	Alkyl	45.2	-16.1	111.6	176.0	10.2
		Acyl	35.0	-27.8	162.3	119.4	

[a] $\Delta\Delta G^{\ddagger} = \Delta G^{\ddagger}_{298}$[Alkyl] – $\Delta G^{\ddagger}_{298}$[Acyl]. Energies are in kcal mol^{-1}.

The reaction barrier for the acyl shift is significantly lower than that for the alkyl shift. In particular, it is lower in sulfite by 12.9 (SO-I) and 10.2 (SO-II) kcal mol^{-1}. Inspection of the transition structures in sulfites reveals that there is a considerably larger degree of angular distortion ($\beta_{TS_{Alkyl}} - \beta_{r_A}$) in alkyl shift (45.3° and 41.8°, entries 2 and 3, Table 3). Although the acyl shift is still more favorable than alkyl shift in phosphoranes, $\Delta\Delta G^{\ddagger}$ is much lower (5.0 kcal mol^{-1}) than that in sulfite. This is clearly supported by the lower difference in angular distortion between alkyl and acyl shifts in phosphorane (19.4° and 24.6°, respectively). It should be noted that the angular distortion in the alkyl shift is lower than that in acyl shift, and this would have led to a lower barrier for the alkyl shift. However, three other factors should be highlighted in order to explain the lower barrier for the acyl shift. First, a higher $\alpha_{TS_{Acyl}}$ (176.4° vs. 168.4° for $\beta_{TS_{Alkyl}}$), which provides better alignment of orbitals between C3—C4 and C2—O1 bonds and higher stability of TS_{Acyl}. Second, the higher stability of conformer A (by 2.7 kcal mol^{-1}) over conformer B (Table 1, entry 2). Unlike the case in sulfites, in phosphorane the energy difference between conformers A and B (2.7 kcal mol^{-1}) is quite significant (> 50%) relative to the difference in barrier heights between the two shifts (5.0 kcal mol^{-1}). Third, the significantly higher migrating C3—C5 bond stretch (1.965 Å) in $TS_{N\text{-}Alkyl}$ compared to C3—C4 (1.780 Å) in

TS_{Acyl} (Table 3). Finally, a relatively short C3—O6 bond distance of 1.262 Å suggests a later TS for the alkyl shift in phosphorane and agrees with its lower exothermicity.

Table 3. Torsion Angles Difference (Angular Distortion) and Bond Lengths in TS Structures.

	X	Shift	Degree of Angular Distortion[a]		Bond Lengths in TS Structure[b]		
			$\alpha_{TS_{Acyl}} - \alpha_{r_B}$	$\beta_{TS_{Alkyl}} - \beta_{r_A}$	C3—C4	C3—C5	C3—O6
1	Ph_3P	Alkyl		19.4	1.559	1.965	1.262
		Acyl	24.6		1.780	1.584	1.285
2	SO-I	Alkyl		45.3	1.545	1.908	1.293
		Acyl	13.7		1.857	1.552	1.306
3	SO-II	Alkyl		41.8	1.540	1.916	1.295
		Acyl	12.8		1.859	1.551	1.308

[a] The degree of angular distortion between the reactant and TS is taken as the difference between the torsion angles in TS and corresponding reactant conformer.
[b] Bond lengths are in Å.

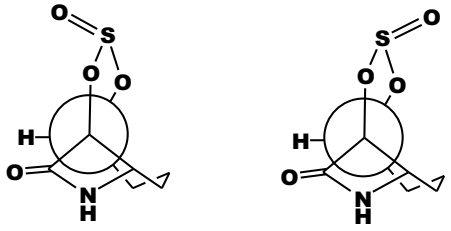

Figure 5. Diastereomers of Sulfite (Conformer B) that Have been Experimentally Shown to Exhibit Different Rates of Semipinacol Rearrangement.[4]

Interestingly, Grainger *et al.* have also reported different rearrangement conversion rates for diastereomers of sulfite. These diastereomers are shown in Figure 5. Our calculations support Grainger's observation of SO-II slower conversion by having SO-II acyl shift barrier 1.2 kcal mol^{-1} higher than that of SO-I. In order to gain more insight into the reactivity of the sulfite isomers, NBO analysis was performed. In particular, we examine the donor-acceptor interaction between lone pairs of O6 and the migrating bond. As shown in Table 4 for SO-I, the $n_{O6} \rightarrow \sigma^*_{C3-C4}$ stabilization energy in conformers A and B combined is higher than that of $n_{O6} \rightarrow \sigma^*_{C3-C5}$. In addition, the $n_{O6} \rightarrow \sigma^*_{C3-C4}$ energy is also higher in TS_{Acyl} than $n_{O6} \rightarrow \sigma^*_{C3-C5}$ in

TS_{Alkyl}. The former and later support the reaction selectivity towards acyl shift via a facilitated C3—C5 bond cleavage and TS_{Acyl} stabilization, respectively. The difference is even more profound compared to $n_{O6} \rightarrow \sigma^*_{C3-C4}$ in SO-II. A much lower $n_{O6} \rightarrow \sigma^*_{C3-C4}$ stabilization energy in SO-II can contribute to its higher acyl-shift barrier. Interestingly, the $n_{O6} \rightarrow \sigma^*_{C3-C5}$ stabilization energies in SO-II are considerably higher than in SO-I; a factor that can similarly explain the 1.5 kcal mol^{-1} lower alkyl shift barrier in SO-II (Table 2).

Table 4. $n \rightarrow \boldsymbol{\sigma}^*$ Stabilization Energy Determined from NBO Analysis (kcal mol^{-1}).

X	$n_{O6} \rightarrow \sigma^*_{C3-C4}$			$n_{O6} \rightarrow \sigma^*_{C3-C5}$		
	Conformer A	**Conformer B**	**TS_{Acyl}**	**Conformer A**	**Conformer B**	**TS_{Alkyl}**
SO-I	9.24	5.91	8.75	3.12	6.52	5.60
SO-II	3.74	2.06	2.70	8.66	8.92	7.64

Although the acyl shift pathway seems to be generally favored in semipinacol rearrangements,[3] alkyl shift is well-known to occur in systems lacking the acyl group.[1,2] Therefore, it is desirable to find a system that can undergo a reversed selectivity and favor the alkyl over the acyl shift. To explore this possibility, we investigated the rearrangement pathways of both phosphorane and sulfite systems derived from the trans-diol isomer shown in Figure 6. Figure 7 illustrates the comparison between the structures of trans- and cis-diol derivatives. In Figure 8 different conformers of trans-diol and their relative energies are shown, whereas Figure 9 summarizes the reaction energies and barrier heights for the trans-diol system. As per the optimized structures of the trans-diol isomer, we expect that it will not only have a relaxed access to TS_{Alkyl}, but also have its TS_{Acyl} structurally inaccessible. This is due to the proper anti-periplanar alignment between O1—C2 and C3—C5 bonds (β_r = 176°) found initially in the optimized structure of the starting adduct (Figure 7 and Figure 8), and the cis arrangement of

O1—C2 and C3—C4 on the cyclohexane ring that makes their anti-periplanar arrangement not possible, respectively. Our calculations show that the diequatorial conformer (Figure 8) that corresponds to the alkyl shift pathway is 2.4 kcal mol^{-1} lower in energy than the diaxial conformer. In addition, the phosphorane and sulfite derivatives of the trans-diol isomer would be conformationally locked in the diequatorial conformer which is just suitable for alkyl shift. Interestingly, our calculations show a pronounced drop in the alkyl shift barrier (by 8–10 kcal mol^{-1}) in trans-diol derivatives compared to those in the cis-diol adducts. The alkyl shift of the proposed trans-diol structure is predicted to be even faster and more exothermic than the acyl shift of the cis-diol in the case of phosphorane (Figure 9).

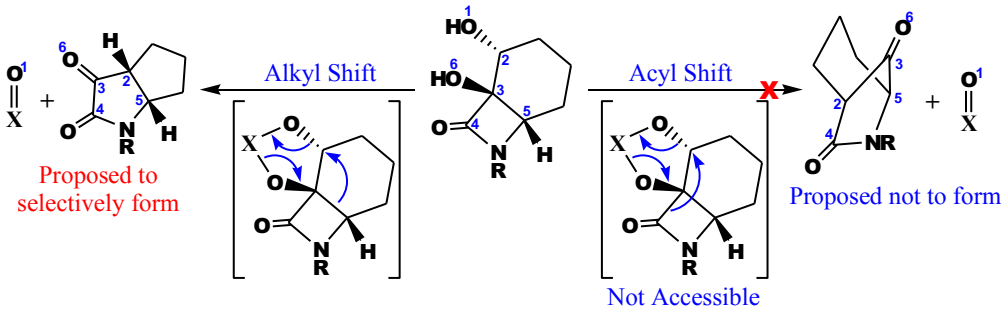

Figure 6. Predicted Selective Semipinacol Rearrangement through Alkyl Shift in a Proposed Trans-Diol System.

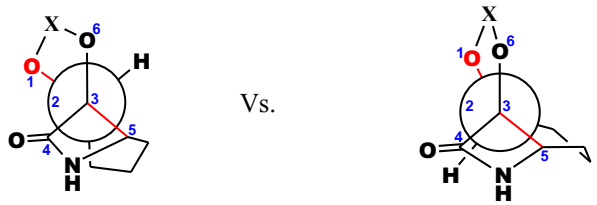

Trans-Diol Derivative

β_r(O1C2C3C5) = 176°

Cis-Diol Derivative (Conformer A)

β_r (O1C2C3C5) = 130-150°

Figure 7. Comparison between Trans and Cis-Diol Derivatives Structural Proximity to TS_{Alkyl} ($\boldsymbol{\beta_{TS_{Alkyl}}}$ = 167-176°).

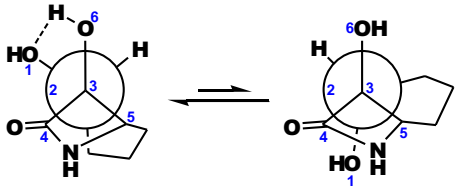

Diequatorial
0.0

Diaxial
2.4

Figure 8. Staggered Conformers of Trans-Diol. Energies are in kcal mol^{-1}. The Diequatorial Conformer Adopts a Syn-Arrangement of the Hydroxyl Groups for which the Formation of Phosphorane or Sulfite Locks it in this Conformer. The Diaxial Conformer Adopts an Anti-Arrangement of the Hydroxyl Groups for which the Formation of Phosphorane and Sulfite Adducts is Obstructed.

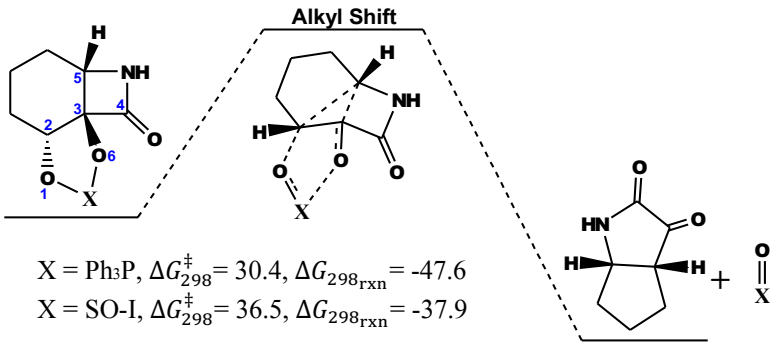

Figure 9. Reaction Energies for the Predicted Selective Alkyl Shift of the Proposed Trans-Diol Derivatives in kcal mol^{-1}.

Conclusions

A high-level computational study using DHDFT methods has been performed in order to examine the selectivity towards acyl migration in the semipinacol rearrangement of cis-fused β-lactam diols. We show that the acyl shift is both kinetically and thermodynamically preferred over the alkyl shift. These results are consistent with previous experimental findings, which show selective acyl migration. Our detailed structural and conformational analysis sheds light on the geometric and orbital-interaction factors that underline this remarkable selectivity. We proceed to show that trans-diol derivative would undergo reversed selectivity favoring the alkyl migration. We hope that this computational prediction would be tested experimentally.

Acknowledgments

This research was undertaken with the assistance of resources from the National Computational Infrastructure (NCI), which is supported by the Australian Government. We also acknowledge

the system administration support provided by the Faculty of Science at the University of Western Australia to the Linux cluster of the Karton group. A.K. gratefully acknowledges an Australian Research Council (ARC) Future Fellowship (Project No. FT170100373).

Supplementary data

Additional potential energy surfaces of semipinacol rearrangements in cis- and trans-fused β-lactam diols (Figures S1–S5); optimized geometries for all the species considered in the present work (Table S1); absolute energies for all the species considered in the present work (Table S2).

References

[1] Gao, A. X.; Thomas, S. B.; Snyder, S. A. Part I: 1,2-Migrations. In *Molecular Rearrangements in Organic Synthesis*; Rojas, C. M., Ed.; Wiley: New York, **2015**; p 15.

[2]Song, Z. –L.; Fan, C. –A.; Tu, Y. –Q. *Chem. Rev.* ***2011****, 111, 7523.*

[3]Alcaide, B.; Almendros, P.; Luna, A.; Cembellin, S.; Arno, M.; Domingo, L. R. *Chem. Eur. J.* **2011**, 17, 11559. Dake, G. R.; Fenster, M. D. B.; Hurley, P. B.; Patrick, B. O. *J. Org. Chem.* **2004**, 69, 5668. Paquette, L. A.; Brand, S.; Behrens, C. *J. Org. Chem.* **1999,** *64,* 2010. Alcaide, B.; Almendros, P.; Luna, A.; Torres, R. M. *Adv. Synth. Catal.* **2010**, 352, 621. Nakamura, E. Kuwajima, I. *J. A,. Chem. Soc.* **1977**, 99, 961. Betou, M.; Male, L.; Steed, J. W.; Grainger, R. S. *Chem. Eur. J.* **2014**, 20, 6505.

[4] Grainger, R. S.; Betou, M.; Male, L.; Pitak, M. B.; Coles, S. J. *Org. Lett.* **2012**, 14, 2234.

[5] Lee, C.; Yang, W.; Parr, R. G. *Phys. Rev. B* **1988**, 37, 785.

[6] Becke, A. D.; *J. Chem. Phys.* **1993**, 98, 5648.

[7] Stephens, P. J.; Devlin, F. J.; Chabalowski, C. F.; Frisch, M. J. *J. Phys. Chem.* **1994**, 98, 11623.

[8] Krishnan, R.; Binkley, J. S.; Seeger, R.; Pople, J. A.; *J. Chem. Phys.* **1980**, 72, 650.

[9] Pople, J. A.; Head-Gordon, M.; Raghavachari, K. *J. Chem. Phys.* **1987**, 87, 5968.

[10] Grimme, S.; Antony, J.; Ehrlich, S.; Krieg, H. *J. Chem. Phys.* **2010**, 132, 154104.

[11] Grimme, S. *WIREs Comput. Mol. Sci.* **2011**, 1, 211.

[12] Becke, A. D.; Johnson, E. R.; *J. Chem. Phys.* **2005**, 123, 154101.

[13] Grimme, S.; Ehrlich, S.; Goerigk, L. *J. Comput. Chem.* **2011**, 32, 1456.

[14] Marenich, A. V.; Cramer, C. J.; Truhlar, D. G.; *J. Phys. Chem. B* **2009**, 113, 6378.

[15] Gonzalez, C.; Schlegel, H. B. *J. Chem. Phys.* **1989**, 90, 2154.

[16] Gonzalez, C.; Schlegel, H. B. *J. Chem. Phys.* **1990**, 94, 5523.

[17] Goerigk, L.; Grimme, S. *WIREs Comput. Mol. Sci.* **2014**, 4, 576.

[18] Kozuch, S.; Martin, J. M. L. *J. Comput. Chem.* **2013**, 34, 2327.

[19] Kozuch, S.; Martin, J. M. L. *Phys. Chem. Chem. Phys.* **2011**, 13, 20104.

[20] Karton, A.; Tarnopolsky, A.; Lamere, J.-F.; Schatz, G. C.; Martin, J. M. L. *J. Phys. Chem. A* **2008**, 112, 12868.

[21] Tarnopolsky, A.; Karton, A.; Sertchook, R.; Vuzman, D.; Martin, J. M. L. *J. Phys. Chem. A* **2008**, 112, 3.

[22] Karton, A.; O'Reilly, R. J.; Radom, L. *J. Phys. Chem. A* **2012**, 116, 4211.

[23] Goerigk, L.; Karton, A.; Martin, J. M. L.; Radom, L. *Phys. Chem. Chem. Phys.* **2013**, 15, 7028.

[24] Karton, A.; Goerigk, L. *J. Comput. Chem.* **2015**, 36, 622.

[25] Yu, L.-J.; Sarrami, F.; O'Reilly, R. J.; Karton, A. *Chem. Phys.* **2015**, 458, 1.

[26] Karton, A.; Sylvetsky, N.; Martin, J. M. L. *J. Comput. Chem.* **2017**, 38, 2063.

[27] Weigend, F.; Ahlrichs, R.; *Phys. Chem. Chem. Phys.* **2005**, 7, 3297.

[28] Curtiss, L. A.; Redfern, P. C.; Raghavachari, K. *J. Chem. Phys.* **2007**, 127, 124105.

[29] Curtiss, L.A.; Redfern, P.C.; Raghavachari, K. *WIREs Comput. Mol. Sci.* **2011**, 1, 810.

[30] Zhao, Y.; Schultz, N. E.; Truhlar, D. G. *J. Chem. Theory Comput.* **2006**, 2, 364.

[31] Frisch, M. J.; Trucks, G. W.; Schlegel, H. B.; Scuseria, G. E.; Robb, M. A.; Cheeseman, J. R.; Scalmani, G.; Barone, V.; Mennucci, B.; Petersson, G. A.; Nakatsuji, H.; Caricato, M.; Li, X.; Hratchian, H. P.; Izmaylov, A. F.; Bloino, J.; Zheng, G.; Sonnenberg, J. L.; Hada, M.; Ehara, M.; Toyota, K.; Fukuda, R.; Hasegawa, J.; Ishida, M.; Nakajima, T.; Honda, Y.; Kitao, O.; Nakai, H.; Vreven, T.; Montgomery, J. A., Jr.; Peralta, J. E.; Ogliaro, F.; Bearpark, M.; Heyd, J. J.; Brothers, E.; Kudin, K. N.; Staroverov, V. N.; Kobayashi, R.; Normand, J.; Raghavachari, K.; Rendell, A.; Burant, J. C.; Iyengar, S. S.; Tomasi, J.; Cossi, M.; Rega, N.; Millam, N. J.; Klene, M.; Knox, J. E.; Cross, J. B.; Bakken, V.; Adamo, C.; Jaramillo, J.; Gomperts, R.; Stratmann, R. E.; Yazyev, O.; Austin, A. J.; Cammi, R.; Pomelli, C.; Ochterski, J. W.; Martin, R. L.; Morokuma, K.; Zakrzewski, V. G.; Voth, G. A.; Salvador, P.; Dannenberg, J. J.; Dapprich, S.; Daniels, A. D.; Farkas, O.; Foresman, J. B.; Ortiz, J. V.; Cioslowski, J.; Fox, D. J. Gaussian 09, Revision D.01; Gaussian, Inc., Wallingford CT, 2009.

[32] Gaussian 16, Revision A.03, Frisch, M. J.; Trucks, G. W.; Schlegel, H. B.; Scuseria, G. E.; Robb, M. A.; Cheeseman, J. R.; Scalmani, G.; Barone, V.; Petersson, G. A.; Nakatsuji, H.; Li, X.; Caricato, M.; Marenich, A. V.; Bloino, J.; Janesko, B. G.; Gomperts, R.; Mennucci, B.; Hratchian, H. P.; Ortiz, J. V.; Izmaylov, A. F.; Sonnenberg, J. L.; Williams-Young, D.; Ding, F.; Lipparini, F.; Egidi, F.; Goings, J.; Peng, B.; Petrone, A.; Henderson, T.; Ranasinghe, D.; Zakrzewski, V. G.; Gao, J.; Rega, N.; Zheng, G.; Liang, W.; Hada, M.; Ehara, M.; Toyota, K.; Fukuda, R.; Hasegawa, J.; Ishida, M.; Nakajima, T.; Honda, Y.; Kitao, O.; Nakai, H.; Vreven, T.; Throssell, K.; Montgomery, J. A., Jr.; Peralta, J. E.; Ogliaro, F.; Bearpark, M. J.; Heyd, J. J.; Brothers, E. N.; Kudin, K. N.; Staroverov, V. N.; Keith, T. A.; Kobayashi, R.; Normand, J.;

Raghavachari, K.; Rendell, A. P.; Burant, J. C.; Iyengar, S. S.; Tomasi, J.; Cossi, M.; Millam, J. M.; Klene, M.; Adamo, C.; Cammi, R.; Ochterski, J. W.; Martin, R. L.; Morokuma, K.; Farkas, O.; Foresman, J. B.; Fox, D. J. Gaussian, Inc., Wallingford CT, 2016.